Engineering 7 (2021) 647–654

Contents lists available at ScienceDirect

Engineering

journal homepage: www.elsevier.com/locate/eng

Research
Green Chemical Engineering: Soft Matter—Article

Engineering the Thermoelectrical Properties of PEDOT:PSS by Alkali Metal Ion Effect

Jingjin Dong [a], Jian Liu [a], Xinkai Qiu [a,b], Ryan Chiechi [a,b], L. Jan Anton Koster [a], Giuseppe Portale [a,*]

[a] Zernike Institute for Advanced Materials, University of Groningen, Groningen 9747 AG, the Netherlands
[b] Stratingh Institute for Chemistry, University of Groningen, Groningen 9747 AG, the Netherlands

ARTICLE INFO

Article history:
Received 31 August 2020
Revised 5 December 2020
Accepted 8 February 2021
Available online 7 May 2021

Keywords:
PEDOT:PSS
Thermoelectric properties
Alkali base solutions
Post-treatment
Structure–property relationship
Grazing-incidence wide-angle X-ray scattering

ABSTRACT

Engineering the electrical properties of poly(3,4-ethylenedioxythiophene):poly(styrenesulfonate) (PEDOT:PSS) holds great potential for various applications such as sensors, thermoelectric (TE) generators, and hole transport layers in solar cells. Various strategies have been applied to achieve optimal electrical properties, including base solution post-treatments. However, the working mechanism and the exact details of the structural transformations induced by base post-treatments are still unclear. In this work, we present a comparative study on the post-treatment effects of using three common and green alkali base solutions: namely LiOH, NaOH, and KOH. The structural modifications induced in the film by the base post-treatments are studied by techniques including atomic force microscopy, grazing-incidence wide-angle X-ray scattering, ultraviolet–visible–near-infrared spectroscopy, and attenuated total reflectance Fourier-transform infrared spectroscopy. Base-induced structural modifications are responsible for an improvement in the TE power factor of the films, which depends on the basic solution used. The results are explained on the basis of the different affinity between the alkali cations and the PSS chains, which determines PEDOT dedoping. The results presented here shed light on the structural reorganization occurring in PEDOT:PSS when exposed to high-pH solutions and may serve as inspiration to create future pH-/ion-responsive devices for various applications.

1. Introduction

Organic electronic (OE) materials have recently attracted increasing interest from the scientific community [1–3]. Due to their flexibility and lightweight properties, they hold great potential in a broad range of applications such as wearable sensors and artificial skins [4–6]. However, it is important to tune and control the properties of these materials in order to prepare ideal devices for different applications [7,8]. Poly(3,4-ethylenedioxy thiophene):poly(styrenesulfonate) (PEDOT:PSS; structure shown in Fig. 1) has been extensively studied among various other OE materials, as it exhibits excellent processability and mechanical and electrical properties [9,10]. One of the hottest application fields is thermoelectrics (TEs), due to the potential for energy harvesting in daily life. The efficiency of TE devices is determined by the so-called "figure of merit (ZT)," $ZT = (\sigma S^2 T)/\kappa$ [11,12], where σ is the electrical conductivity, S is the Seebeck coefficient, κ is the thermal conductivity, and T is the absolute temperature. For polymers, the co-called power factor (PF), where $PF = \sigma S^2$, is the main aspect to improve due to the intrinsically low thermal conductivity of polymeric TE materials [13,14].

Polar solvents with a high boiling point were first found to be able to enhance the electrical properties of PEDOT:PSS when used as additives or as post-treatment solvents [2,15,16]. For example, the addition of dimethyl sulfoxide (DMSO) into PEDOT:PSS films enhances phase separation and triggers the formation of interconnected networks of crystalline elongated PEDOT domains. This leads to a great enhancement of σ (from originally ~10^0 S·cm^{-1} to an optimized ~10^3 S·cm^{-1}) without compromising S [17]. On the basis of DMSO addition, Lee et al. [18] applied a dedoping process by over-coating a strong reducing agent such as hydrazine onto PEDOT:PSS nanofilms, which led to an enhanced Seebeck coefficient and PF (σ = 578 S·cm^{-1}, S = 67 μV·K^{-1}, PF = 259 μW·m^{-1}·K^{-2}). Fan et al. [19] introduced sequential post-treatments with H_2SO_4 and NaOH on PEDOT:PSS thin film. After

* Corresponding author.
E-mail address: g.portale@rug.nl (G. Portale).

https://doi.org/10.1016/j.eng.2021.02.011

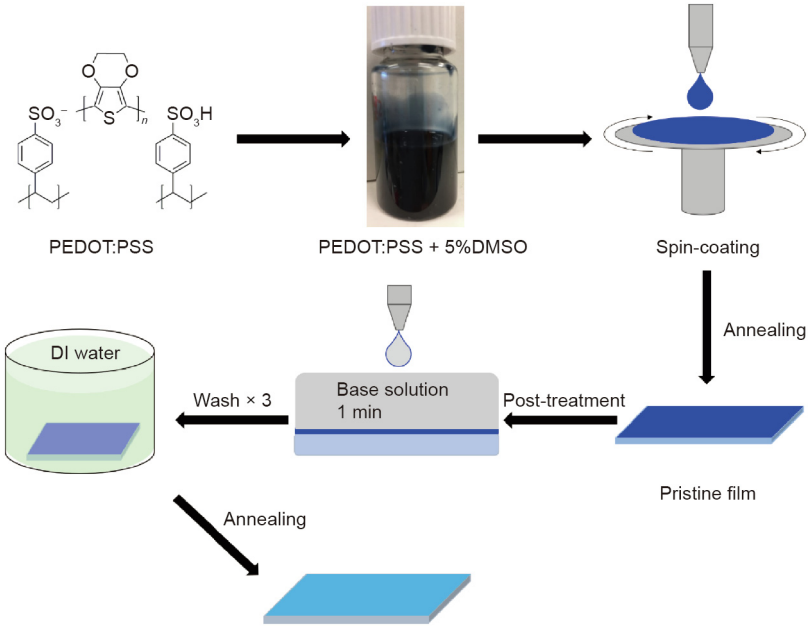

Fig. 1. Materials, fabrication, and post-treatment process employed here to prepare the PEDOT:PSS thin films. DI: deionized; DMSO: dimethyl sulfoxide.

the acid treatment, σ increased dramatically to 2000–3000 $S \cdot cm^{-1}$ due to the sufficient removal of PSS, and subsequently formed nanosized fibrous structures that significantly promoted the charge mobility in the film. It was shown that the base treatment induces a low oxidation level of PEDOT and thus improves the Seebeck coefficient. Although σ was found to decrease during the base treatment, an optimized PF of 334 $\mu W \cdot m^{-1} \cdot K^{-2}$ was obtained. These results showed that larger PFs can be achieved by first improving the electrical conductivity by morphology and structure modification, and then increasing the Seebeck coefficient by lowering the oxidation state of PEDOT. Moreover, the results proved the dependence of the post-treatment agents' pH on TE performance. While acid treatment has been well studied due to its positive effect on electrical conductivity [20–23], a detailed study on base post-treatment is still lacking, especially one involving the use of different cations. Unanswered questions are: Do certain cations have an effect on performance, even when samples are exposed to a solution with the same pH? If so, what is the mechanism behind the performance change?

In this work, a very easy and environmentally friendly process is applied to tune the TE properties of PEDOT:PSS. Three different alkali base solutions (LiOH, NaOH, and KOH dissolved in deionized (DI) water) are used as post-treatment agents for pristine PEDOT:PSS:DMSO thin films deposited by means of spin-coating (Fig. 1). To allow a comparison, the same concentration of 1 $mol \cdot L^{-1}$ is used at first, which means that the anions and cations can fully dissociate and the pH of each the solution is the same [24–26]. Electrical conductivity and Seebeck coefficient are probed to determine the film performances, and a series of characterization methods including atomic force microscopy (AFM), grazing-incidence wide-angle X-ray scattering (GIWAXS), ultraviolet–visible–near-infrared (UV-vis-NIR) spectroscopy, and attenuated total reflectance Fourier-transform infrared (ATR-FTIR) spectroscopy are used to study the effect of the alkali solution treatment on the PEDOT:PSS structure. Furthermore, different solution concentrations are used to obtain a database for tuning the TE properties and for other potential applications.

2. Results and discussion

2.1. TE properties

The TE properties measured for the pristine film and for the films post-treated with LiOH, NaOH, and KOH solutions are reported in Fig. 2 (films are referred to as LiOH_PT, NaOH_PT, and KOH_PT in the following). As expected, the σ decreases upon treatment with alkaline solutions, while the S increases compared with the pristine film. However, a clear trend is observed for both the σ and S of the post-treated films depending on the kind of cation used (i.e., cations of different size). The larger the cation size, the lower the σ and the higher the S. σ drops significantly from 600 $S \cdot cm^{-1}$ in the pristine film to 244, 201, and 184 $S \cdot cm^{-1}$ in the LiOH, NaOH, and KOH post-treated films, respectively. At the same time, S undergoes a dramatic increase from the initial value of 15.0 to 20.9, 37.8 $\mu V \cdot K^{-1}$ and, finally, 51.9 $\mu V \cdot K^{-1}$. Considering that the pH of the different solutions is identical, we speculate that the main impact on the TE properties is the cation nature, as discussed below. As a result of the dramatic increase in S, the calculated PF also shows an increasing trend from LiOH_PT to KOH_PT (Fig. 2(b)). Notably, the KOH_PT film exhibits an optimized value of about 50.0 $\mu W \cdot m^{-1} \cdot K^{-2}$, which is almost two times higher than the value for the pristine PEDOT:PSS:DMSO film, and which is competitive with the results from many other complex engineering methods [14].

2.2. Surface morphology and crystalline structure

We further investigated the relationship between the properties and structure of the treated films using microscopy and GIWAXS. At first, the large-scale film homogeneity of the films was tested using optical microscopy (OM). All the films showed a homogeneous structure without any significant large-scale inhomogeneity. As an example, we report the OM images for the KOH_PT sample (Fig. S1 in Appendix A). The surface structure was then measured by AFM. The height and phase images of the studied films were

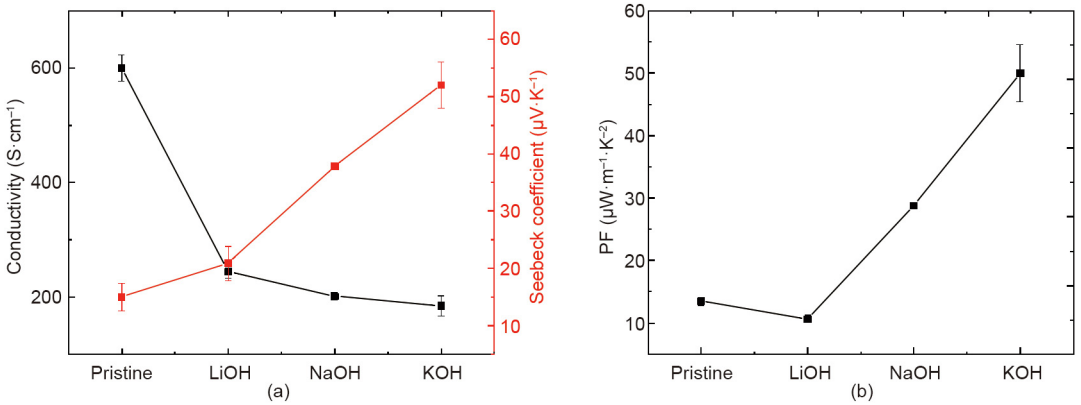

Fig. 2. TE properties of the different PEDOT:PSS:DMSO thin films post-treated using different basic solutions: (a) conductivity and Seebeck coefficient together with (b) the calculated PF. The concentration is maintained at 1 mol·L^{-1}.

captured using tapping mode AFM and are summarized in Fig. 3. We observed interconnected networks of PEDOT crystals (which appear as elongated grains in Fig. 3(a)) in the pristine PEDOT:PSS:DMSO film in both the height and phase images, which is in good agreement with the literature [17]. These interconnected networks are barely visible on the films that were post-treated with LiOH (Fig. 3(b)). Instead, we observed circular grains (highlighted in Fig. 3(b)) in both the height and phase images. This morphological transition is also persistent in the films post-treated by NaOH (Fig. 3(c)) and KOH (Fig. 3(d)). The surface roughness values for all the studied films are very similar. The formation of a morphology composed of circular grains in the post-treated films can be rationalized by spherical crystalline PEDOT islands being spatially distributed into the matrix of PSS. The transition from an interconnected PEDOT crystallite network to the isolated crystalline islands observed here corroborates reported observations in localized charge carriers and low carrier mobility due to a shortened mean free path [27]. On the other hand, potential barriers generated from the grain boundaries in post-treated films only allow the transport of high-energy charge carriers to the cold side [28], which explains the increase in the Seebeck coefficient reported in Fig. 2.

The semi-crystalline structure of the pristine and post-treated films was investigated by GIWAXS, as shown in Figs. 4(a)–(d). Similar to the surface morphology, the bulk film crystalline structure undergoes a great change after the post-treatment with base solutions. To better visualize the structural changes, full integration line profiles from the images are reported in Fig. 4(e). The low-angle region features two peaks: the (100) reflection located at the lowest scattering vector ($\boldsymbol{q}$) values and a second peak located at around 0.48 Å^{-1}. Note that the dip caused by the gaps in the Pilatus detector sits in between these two peaks in the full integration profile, as shown in Fig. 4(e). However, these two peaks are clearly visible in the intensity linecuts along the vertical out-of-plane ($\boldsymbol{q}_z$, the near-out-of-plane scattering vector) direction, as shown in Appendix A Fig. S2. It is notable that the (100) peak located around q = 0.24 Å^{-1} for the pristine film decreases in intensity after post-treatment (a decrease of 4%, 20%, and 37% for LiOH, NaOH, and KOH, respectively) and shifts to 0.28, 0.32, and 0.36 Å^{-1}

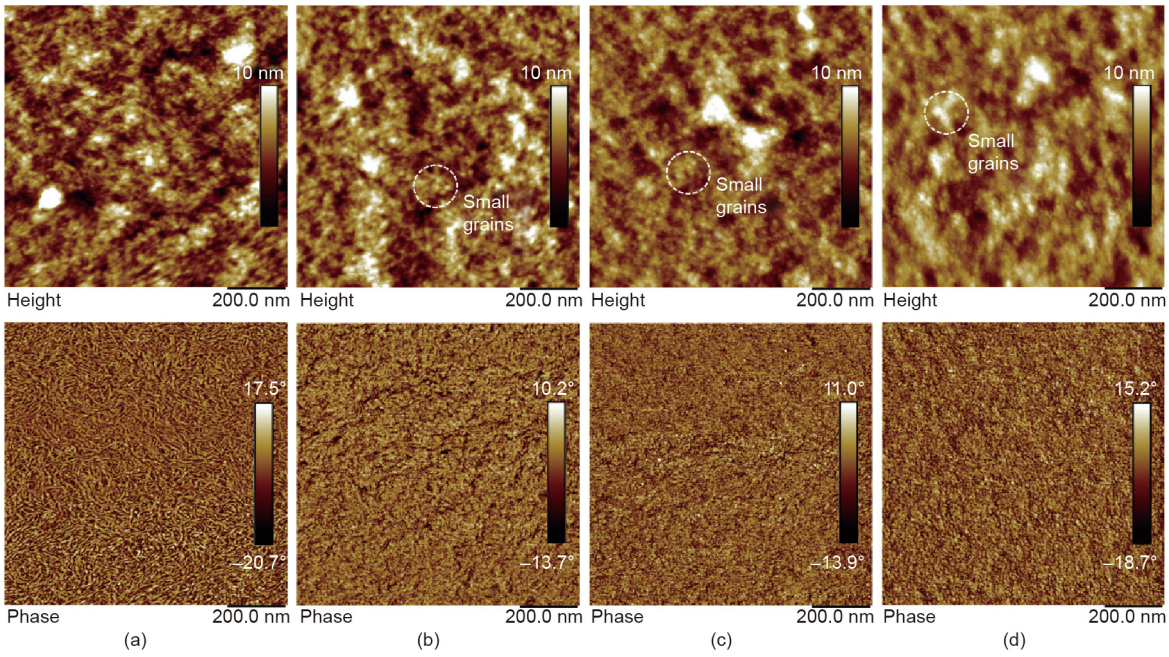

Fig. 3. AFM height (top) and phase (bottom) images of (a) pristine PEDOT:PSS:DMSO films and (b–d) PEDOT:PSS:DMSO films post-treated with (b) LiOH, (c) NaOH, and (d) KOH.

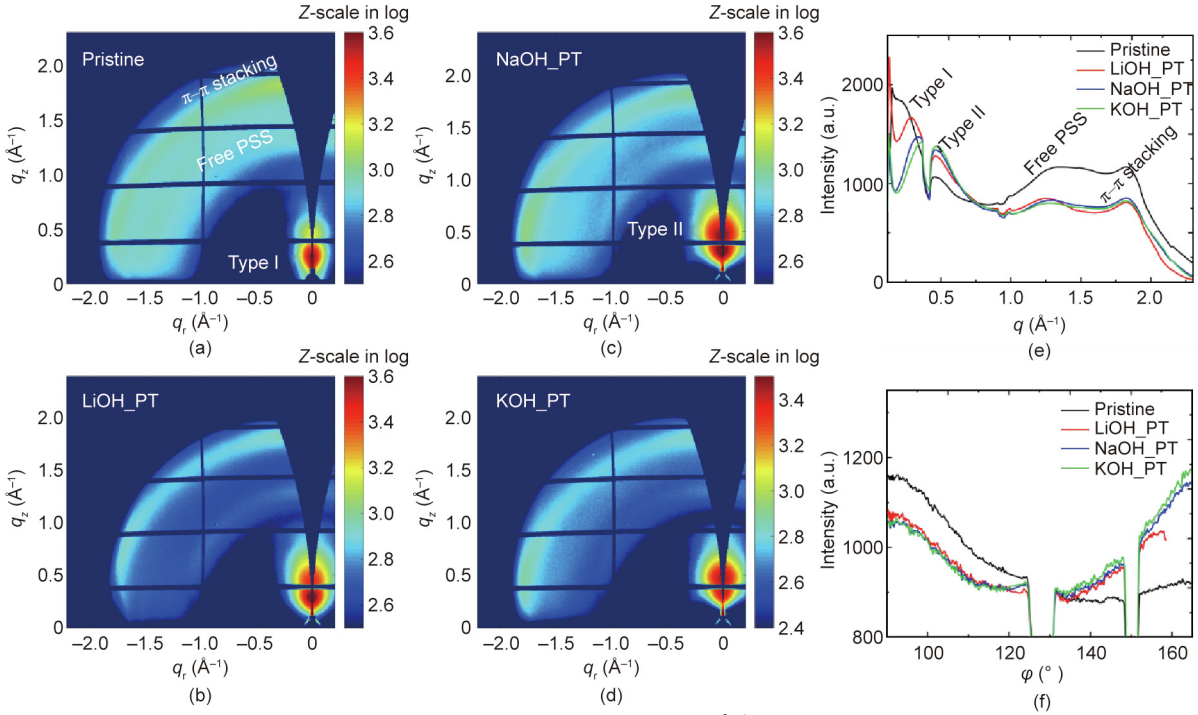

Fig. 4. (a–d) GIWAXS images, (e) full integration line profiles, and (f) peak intensity around q = 1.83 Å^{-1} (PEDOT π–π stacking) against the azimuthal angle (φ) for different base solutions in post-treated PEDOT:PSS:DMSO thin films. The dips in the intensity profiles of parts (e) and (f) are due to the gaps in the Pilatus detector. $\boldsymbol{q}$: the scattering vector; $\boldsymbol{q}_z$: the near-out-of-plane scattering vector; $\boldsymbol{q}_r$: the parallel component of the scattering vector.

for the LiOH_PT, NaOH_PT, and KOH_PT films, respectively. This means that the spacing between adjacent (100) planes becomes increasingly smaller going from the pristine film to the KOH_PT film (from 26.2 to 22.4, 19.6, and 17.4 Å, respectively). This more compact packing along the [100] direction is expected to help the charge carrier transport inside the crystal [29]. The (100) d-spacing (d means the distance between the crystalline planes) for the spin-coated PEDOT:PSS:DMSO films reported here is somehow bigger than what we have previously reported for drop-casting films, indicating that packing differences resulted from these two film-preparation methods [30]. Remarkably, the intensity of the peak located at q = 0.48 Å^{-1} along the q_z direction exhibits a strong increase going from the pristine film to the KOH_PT film. While the (100) peak position clearly shifts with the alkali metal atom used, the position of the peak at q = 0.48 Å^{-1} is almost unchanged. Moreover, the trend in intensity of these two peaks is opposite. These observations suggest that the peak at q = 0.48 Å^{-1} cannot be associated with the second order of the (100) peak, as is usually reported for pristine PEDOT:PSS:DMSO. Indeed, two different types of packing were recently reported by Bießmann et al. [31], each one characterized by a different (100) peak position. Type I PEDOT crystals show sufficiently doped PEDOT chains closely surrounded by PSS and exhibit a larger d-spacing along the [100] direction (a (100) peak located toward smaller q values). In contrast, Type II PEDOT crystals show little or even no PSS inside the PEDOT crystals, making the (100) d-spacing smaller (a (100) peak located toward higher q values). In our case, the PEDOT packing varies from mainly Type I to a mixture of Type I and Type II, depending on the nature of the alkaline solution used (the calculated ratio of Type I to Type II changed from 1.80 to 1.31, 1.10, and 1.05 going from pristine to LiOH_PT, NaOH_PT, and KOH_PT, respectively). This finding indicates the progressive removal of doping PSS from the PEDOT crystallites and, thus, the occurrence of a base-induced dedoping process.

In addition to the change in the PEDOT packing structure, the free PSS chains not directly associated with PEDOT showed changes following the base treatment. The free PSS peak exhibits a clear shift from around 1.32 Å^{-1} for pristine film to 1.24, 1.28, and 1.28 Å^{-1} for LiOH_PT, NaOH_PT, and KOH_PT, respectively. This observation indicates that the alkaline solutions have an interaction with the free PSS inside the films, making the average distance among the PSS chains larger (from 4.8 Å for pristine to 5.1, 4.9, and 4.9 Å for LiOH_PT, NaOH_PT, and KOH_PT, respectively). In contrast, the (010) peak, which is associated with the ordering along the PEDOT π–π stacking direction, remains at the same peak position of around 1.83 Å^{-1}, suggesting that the post-treatment agents do not affect the inner molecular packing distance of the PEDOT chains along the π–π stacking direction. However, changes can be observed in the (010) peak width after post-treatment (Fig. 4(e)). The observed (010) peak broadening is minor for LiOH_PT, but is not negligible for the other two samples. The (010) peak width significantly increases for the NaOH_PT and KOH_PT films, which means that the crystal coherence length along the [010] direction (CCL_{010}) becomes smaller. CCL_{010} changes from 18.5 to 15.7 Å; thus, the average number of π–π stacking layers decreases from 5.4 to 4.5 on average. This loss in crystal quality well explains the observed decrease in film conductivity [30]. Moreover, the (010) peak shows a strong intensity enhancement along the horizontal in-plane q_y direction (indicating edge-on orientation) and a decrease along the vertical near-out-of-plane q_z direction (indicating face-on orientation) upon film post-treatment (see the azimuthal intensity profiles in Fig. 4(f)). The estimated fractions of face-on and edge-on crystals for pristine PEDOT:PSS:DMSO are 53.3% and 12.3%, respectively, while these fractions change to 48.0% and 18.1% for the post-treated samples (values were calculated using the method presented in our previous work [30]). This finding indicates that the base post-treatment promotes a more edge-on orientation of the PEDOT crystallites. This crystal orientation change could partially compensate for the conductivity loss, limiting the drop in σ. Together with the AFM results, the GIWAXS observations clearly reveal that the elongated grains present in the pristine film are formed by heavily

doped PEDOT crystals with preferential face-on orientation, while the smaller globular domains appearing in the post-treated films are formed by less doped (even neutral) smaller PEDOT crystals with a less pronounced orientation, but still mainly with a face-on orientation.

2.3. Electronic structure

UV-vis-NIR absorption spectroscopy was applied to study the oxidation state of the thin films post-treated with the different alkali base solutions. As shown in Fig. 5(a), compared with the pristine PEDOT:PSS:DMSO film, the post-treated films feature a remarkable increase in the signal intensity in the 400–700 and 700–1200 nm wavelength ranges, which represents the neutral and polaron states according to the conventional explanation [32,33]. Concomitantly, the spectra of the post-treated films show a clear intensity decrease in the 1200–1600 nm wavelength region, which represents the bipolaron state. Among the three bases, LiOH_PT and NaOH_PT exhibit quite similar behavior, while KOH_PT shows a much stronger change. These variations are similar to those observed by Stepien et al. [34] for PEDOT:PSS films prepared from a KOH-added solution, and constitute direct evidence of the dedoping process caused by the base solutions. The shrinkage of the bipolaron band and the dissociation of bipolarons into polarons and even neutral species, as observed here, are associated with an upward shift of the Fermi level, far away from the valence band, which makes the material a non-degenerate semi-conductor and well explains the high Seebeck coefficient measured for the post-treated films (Fig. 2(a)) [35,36]. We also note that the interpretation of the PEDOT:PSS UV-vis-NIR spectra has been recently revised. Zozoulenko et al. [37] reported on the basis of density functional theory (DFT) calculations that the peak at 700–1000 nm could be attributed to both polarons and bipolarons, and that the peak in the NIR range could be attributed to polaronic and bipolaronic states coming from PEDOT with a high oxidation level. However, the conclusions drawn here still stand in the view of this new interpretation, as the increasing/decreasing trend in the vis/NIR range supports the variation from a high oxidation state to a low oxidation state after base solution post-treatment.

To further study the effect of the base post-treatment on the chemical structures, ATR-FTIR spectroscopy was employed. As shown in Fig. 5(b), several changes can be observed when comparing the ATR-FTIR spectra of the post-treated films with that of the pristine film. The peak at wavenumber 1155 cm^{-1} decreases dramatically upon base treatment. This signal is associated with the asymmetric S=O stretching of PSS in the proton form, indicating that $-SO_3H$ has changed to $-SO_3^-$ [38]. The increase of the peak at 1524 cm^{-1}, which belongs to the symmetric C_α=C_β stretching of the thiophene ring, and the decrease of the peak at 1557 cm^{-1} (shifted to 1547 cm^{-1}), which belongs to the asymmetric C_α=C_β stretching, together suggest a change in the structure from a more quinoid to a more benzoid structure [39,40]. A red shift from 1263 to 1249 cm^{-1}, which represents the C_α–$C_{\alpha'}$ inter-ring stretching, also suggests that the C_α–$C_{\alpha'}$ bond varied from a more double-bond structure (quinoid) to a single-bond structure (benzoid). All these changes further support the base-induced dedoping process discussed above. Importantly, LiOH_PT exhibited a clear shoulder at the wavenumber 1220 cm^{-1}. This peak can be attributed to the S=O stretching from $-SO_3$-Li^+, indicating a stronger interaction between PSS^- and Li^+. This observation is very important in the light of the discussion about the working mechanism reported below.

2.4. Working principle

According to all the findings discussed above, a possible mechanism can be summarized. As shown in Fig. 6, exposure to a basic solution causes a neutralization reaction to occur, with PSSH changing to PSS^-. At the same time, part of the highly doped PEDOT chains (bipolarons) are reduced (into the polaron state). Due to the different ion sizes, the three alkali ions have a different affinity to PSS^-. As the smallest ion, Li^+ would have the highest affinity, while K^+, as the biggest, would have the lowest affinity. In this situation, we can consider the PSS^- to be an ion-exchange resin. In the next step, washing with DI water removes all the free ions. For KOH_PT, free ions meant that all the K^+ were applied, while for LiOH_PT, some Li^+ still remained inside the PSS matrix. This supposition is evidenced by the PSS peak shift (larger *d*-spacing) shown in GIWAXS and the appearance of the salt-form sulfonate peak in the ATR-FTIR spectrum. To balance the negative charges (i.e., dissociated sulfonate groups in the PSS matrix) caused by the removal of positive ions, the p-type doped PEDOT chains will accept the electrons from the PSS^- and become dedoped. As KOH_PT has the most dissociated sulfonate groups, it is supposed to have the lowest doping state. The difference in ion affinity for the PSS will be particularly true when the interaction is not in the hydrated state [41], as in our case. Fig. S3(a) in Appendix A shows a time evolution of the integrated GIWAXS profiles for a 1 mol·L^{-1} LiOH solution post-treatment process before washing (similar trends are observed for NaOH and KOH). After alkali solution exposure, water

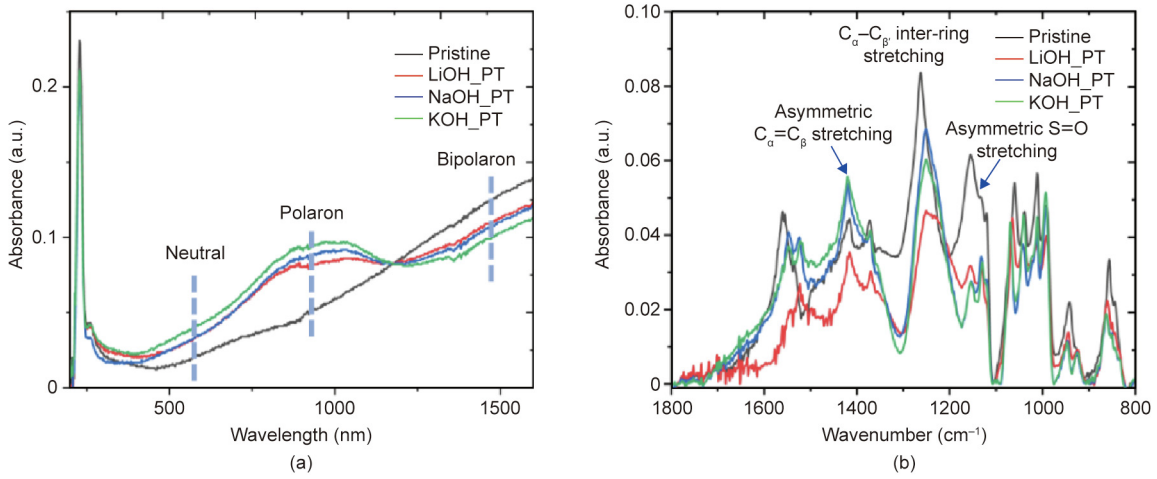

Fig. 5. (a) UV-vis-NIR and (b) ATR-FTIR spectra for PEDOT:PSS:DMSO thin films post-treated with different bases.

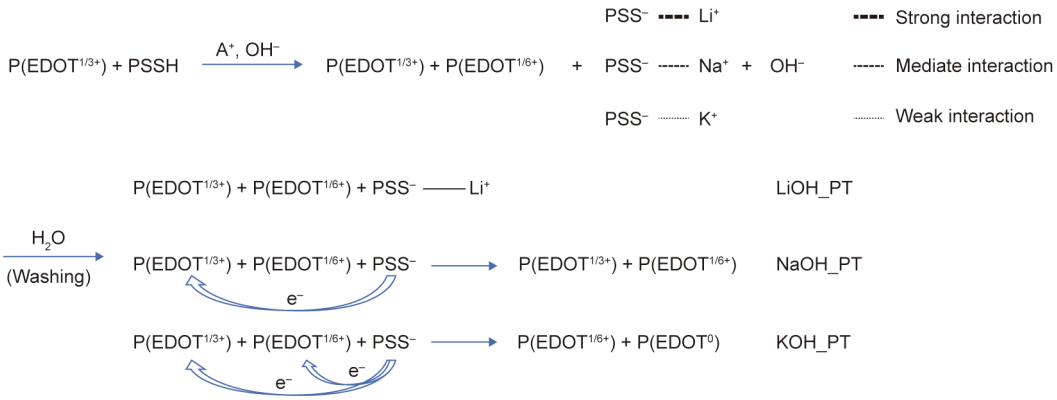

Fig. 6. Proposed mechanism of the alkali base solution post-treatment process for PEDOT:PSS-based thin films. A^+: Li^+, Na^+, or K^+; $P(EDOT^{1/3+})$: bipolaron; $P(EDOT^{1/6+})$: polaron; $P(EDOT^0)$: neutral.

evaporates within the first 5–7 min. Right after the excess liquid droplet is evaporated from the surface of the film (time point t = 420 s), the free PSS^-/Li^+ peak is located at q = 1.25 $Å^{-1}$. Its position does not shift anymore in time until the end of the drying process (t = 1800 s), and the free PSS peak only becomes sharper during drying. Moreover, the sample peak position is recorded after the washing and temperature annealing steps (Fig. 4(e)). The average distance among the PSS chains is around 5.0 Å for LiOH_PT and around 4.9 Å for NaOH_PT and KOH_PT, suggesting that tight nanochannels are present within the free PSS domains, only allowing the diffusion of "dehydrated" cations [41]. The mechanism unveiled here well explains the counterintuitive TE performance difference among the PEDOT:PSS:DMSO films post-treated by bases with the same reducing equivalent but different alkali cations. Our results are in agreement and complement previously published works on the acid-base treatment of PEDOT:PSS [42].

To further confirm this hypothetical mechanism, another three post-treatment agents were also studied. As shown in Fig. 7, PEDOT:PSS:DMSO films post-treated with aqueous LiCl, NaCl, and KCl solutions show a lower electrical conductivity and higher Seebeck coefficient performance than the pristine PEDOT:PSS:DMSO film. However, there is no obvious trend among them. σ remains around 400–500 $S \cdot cm^{-1}$ and S remains around 22.2 $\mu V \cdot K^{-1}$ (Fig. 7(a)). Also, no clear trend is observed for the calculated PF, which oscillates between 23 and 27 $\mu W \cdot m^{-1} \cdot K^{-2}$ (Fig. 7(b)). Moreover, these values are quite close to the value obtained when PEDOT:PSS:DMSO is treated with simple water washing. This observation matches well with our hypothesis of the ion-exchange resin effect, as it strongly depends on the pH [43,44]. While free PSSH can be successfully transformed into PSS^- by the OH^- when exposed to alkali base solutions, the Cl^- ions have a much lower interaction with PSSH, so the ion-exchange resin mechanism does not apply to the salt solution post-treatment. In addition, the experimental observations reported here exclude the energy-filtering effect principle. If one considers the energy-filtering effect to dominate the Seebeck coefficient difference, the trend among the chloride-salt-treated samples is supposed to be for all the base-treated samples. However, this is clearly not the case here [45,46].

2.5. Concentration dependence

In Figs. 8(a)–(c), three TE property maps against both different alkali metal ions and different solution concentrations are shown. With the increase in concentration, σ drops from 600 to 60 $S \cdot cm^{-1}$, and S increases from 16 to 56 $\mu V \cdot K^{-1}$. Notably, when the highest concentration of 5 $mol \cdot L^{-1}$ was used for KOH, the Seebeck coefficient shows a decrease compared with lower concentrations. This can be explained by the fact that the high concentration of the base destroys not only the elongated chain structure, but also the crystallinity, so that the thermal-driven carriers are blocked when moving to the cold side [39,47]. Fig. S4 in Appendix A shows the GIWAXS results of NaOH_PT films post-treated with different concentrations; the revealed structure matches well with the TE properties shown here. The data presented in Fig. 8 highlight the sensitivity of PEDOT:PSS toward the concentration and the nature of the alkali solution.

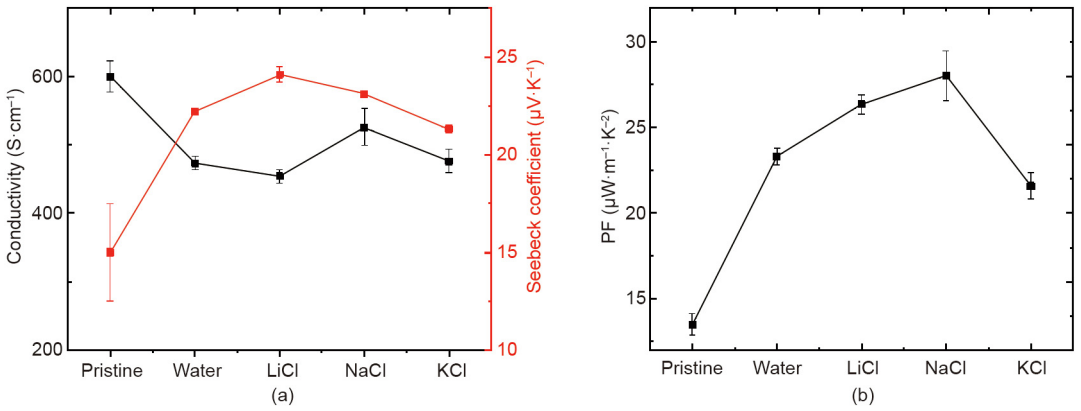

Fig. 7. TE properties of PEDOT:PSS:DMSO thin films post-treated with different salt solutions: (a) conductivity and Seebeck coefficient and (b) PF calculated.

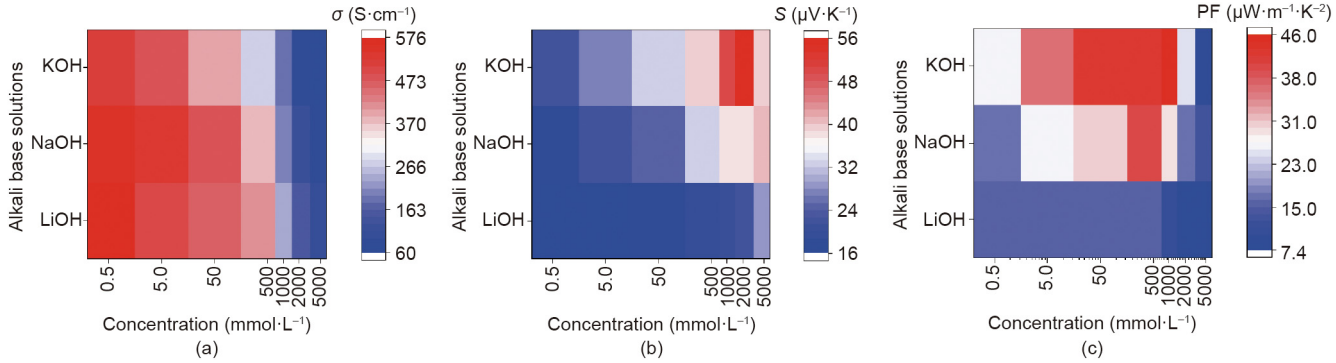

Fig. 8. (a) Electrical conductivity, (b) Seebeck coefficient, and (c) PF of LiOH_PT, NaOH_PT, and KOH_PT films with different post-treatment agent concentrations.

3. Conclusions

In summary, in this paper, we show that the TE performance of PEDOT:PSS thin films can be finely tuned using exposure to different alkali metal ion basic solutions. The post-treatment method explored here is simple and green. Various characterization techniques including AFM, GIWAXS, UV-vis-NIR, and ATR-FTIR were employed to reveal the possible working principle. A series of different post-treatment concentrations was applied, making it possible to reach an optimal PF of 56 $\mu W \cdot m^{-1} \cdot K^{-2}$ when using a 2 $mol \cdot L^{-1}$ KOH solution. Based on the measured TE properties, a database for the electrical conductivity and Seebeck coefficient as a function of the post-processing conditions is presented here.

The changes in the material TE properties are explained using an "ion-exchange resin effect," based on the different affinity between the alkali cations and the PSS^- chains. The alkali metal ion effect reported here could be further explored for potential applications in various fields such as a hole transport layer for solar cells, organic electrochemical transistors, and memristors for neuromorphic devices.

Acknowledgements

The European Synchrotron Radiation Facility (ESRF) and the Dutch Research Council (NWO) are acknowledged for allocating the beam time at the Dutch–Belgian beamline (DUBBLE, ESRF, and Grenoble) for the GIWAXS experiments. The authors are grateful to the DUBBLE team for their help during the beam time. Giuseppe Portale acknowledges the Zernike Institute for Advanced Materials for the startup funds. Jingjin Dong and Giuseppe Portale are grateful to the China Scholarship Council (201606340158).

Compliance with ethics guidelines

Jingjin Dong, Jian Liu, Xinkai Qiu, Ryan Chiechi, Jan Anton Koster, and Giuseppe Portale declare that they have no conflict of interest or financial conflicts to disclose.

Appendix A. Supplementary data

Supplementary data to this article can be found online at https://doi.org/10.1016/j.eng.2021.02.011.

References

[1] Wang Y, Yang L, Shi XL, Shi X, Chen L, Dargusch MS, et al. Flexible thermoelectric materials and generators: challenges and innovations. Adv Mater 2019;31(29):1807916.
[2] McGrail BT, Sehirlioglu A, Pentzer E. Polymer composites for thermoelectric applications. Angew Chem Int Ed Engl 2015;54(6):1710–23.
[3] Liu J, Shi Y, Dong J, Nugraha MI, Qiu X, Su M, et al. Overcoming Coulomb interaction improves free-charge generation and thermoelectric properties for n-doped conjugated polymers. ACS Energy Lett 2019;4(7):1556–64.
[4] Wang Y, Zhu C, Pfattner R, Yan H, Jin L, Chen S, et al. A highly stretchable, transparent, and conductive polymer. Sci Adv 2017;3(3):e1602076.
[5] Rivnay J, Wang H, Fenno L, Deisseroth K, Malliaras GG. Next-generation probes, particles, and proteins for neural interfacing. Sci Adv 2017;3(6):e1601649.
[6] Feig VR, Tran H, Lee M, Bao Z. Mechanically tunable conductive interpenetrating network hydrogels that mimic the elastic moduli of biological tissue. Nat Commun 2018;9(1):2740. Erratum in: Nat Commun 2018;9(1):5030.
[7] Liu J, Ye G, van der Zee B, Dong J, Qiu X, Liu Y, et al. N-type organic thermoelectrics of donor–acceptor copolymers: improved power factor by molecular tailoring of the density of states. Adv Mater 2018;30(44):1804290.
[8] Liu J, Qiu L, Alessandri R, Qiu X, Portale G, Dong J, et al. Enhancing molecular n-type doping of donor–acceptor copolymers by tailoring side chains. Adv Mater 2018;30(7):1704630.
[9] Sun K, Zhang S, Li P, Xia Y, Zhang X, Du D, et al. Review on application of PEDOTs and PEDOT:PSS in energy conversion and storage devices. J Mater Sci Mater Electron 2015;26(7):4438–62.
[10] Zhang B, Sun J, Katz HE, Fang F, Opila RL. Promising thermoelectric properties of commercial PEDOT:PSS materials and their Bi_2Te_3 powder composites. ACS Appl Mater Interfaces 2010;2(11):3170–8.
[11] Bell LE. Cooling, heating, generating power, and recovering waste heat with thermoelectric systems. Science 2008;321(5895):1457–61.
[12] Tritt TM, Subramanian MA. Thermoelectric materials, phenomena, and applications: a bird's eye view. MRS Bull 2006;31(3):188–98.
[13] Bubnova O, Crispin X. Towards polymer-based organic thermoelectric generators. Energy Environ Sci 2012;5(11):9345–62.
[14] Zhu Z, Liu C, Jiang F, Xu J, Liu E. Effective treatment methods on PEDOT:PSS to enhance its thermoelectric performance. Synth Met 2017;225:31–40.
[15] Liu S, Deng H, Zhao Y, Ren S, Fu Q. The optimization of thermoelectric properties in a PEDOT:PSS thin film through post-treatment. RSC Adv 2015;5(3):1910–7.
[16] Kim GH, Shao L, Zhang K, Pipe KP. Engineered doping of organic semiconductors for enhanced thermoelectric efficiency. Nat Mater 2013;12(8):719–23.
[17] Luo J, Billep D, Waechtler T, Otto TW, Toader M, Gordan OD, et al. Enhancement of the thermoelectric properties of PEDOT:PSS thin films by post-treatment. J Mater Chem A 2013;1(26):7576–83.
[18] Lee SH, Park H, Kim S, Son W, Cheong IW, Kim JH. Transparent and flexible organic semiconductor nanofilms with enhanced thermoelectric efficiency. J Mater Chem A 2014;2(20):7288–94.
[19] Fan Z, Li P, Du D, Ouyang J. Significantly enhanced thermoelectric properties of PEDOT:PSS films through sequential post-treatments with common acids and bases. Adv Energy Mater 2017;7(8):1602116.
[20] Lee JH, Jeong YR, Lee G, Jin SW, Lee YH, Hong SY, et al. Highly conductive, stretchable, and transparent PEDOT:PSS electrodes fabricated with triblock copolymer additives and acid treatment. ACS Appl Mater Interfaces 2018;10(33):28027–35.
[21] Ouyang J. Solution-processed PEDOT:PSS films with conductivities as indium tin oxide through a treatment with mild and weak organic acids. ACS Appl Mater Interfaces 2013;5(24):13082–8.
[22] McCarthy JE, Hanley CA, Brennan LJ, Lambertini VG, Gun'Ko YK. Fabrication of highly transparent and conducting PEDOT:PSS films using a formic acid treatment. J Mater Chem C 2014;2(4):764–70.
[23] Mengistie DA, Ibrahem MA, Wang PC, Chu CW. Highly conductive PEDOT:PSS treated with formic acid for ITO-free polymer solar cells. ACS Appl Mater Interfaces 2014;6(4):2292–9.
[24] Sodium hydroxide solution [Internet]. Shanghai: Sigma-Aldrich LLC; c2021 [cited 2020 Aug 31]. Available from: https://www.sigmaaldrich.com/catalog/product/mm/109137?lang=en&region=NL.

[25] Potassium hydroxide solution, 0.1M, Chem-Lab [Internet]. Porto: Thermo Fisher Scientific; c2021 [cited 2020 Aug 31]. Available from: https://www.fishersci.pt/shop/products/potassium-hydroxide-0-1n-20/11933193.
[26] Saario T, Tähtinen S. *In situ* measurement of tee effect of LiOH on the stability of zircaloy-2 surface film in PWR water. In: Proceedings of IAEA Technical Committee Meeting on Influence of Water Chemistry on Fuel Cladding Behaviour; 1993 Oct 4–8; Rez, Czech Republic; 1993.
[27] Saeki A, Koizumi Y, Aida T, Seki S. Comprehensive approach to intrinsic charge carrier mobility in conjugated organic molecules, macromolecules, and supramolecular architectures. Acc Chem Res 2012;45(8):1193–202.
[28] Lu J, Guo R, Dai W, Huang B. Enhanced in-plane thermoelectric figure of merit in p-type SiGe thin films by nanograin boundaries. Nanoscale 2015;7(16):7331–9.
[29] Shi W, Zhao T, Xi J, Wang D, Shuai Z. Unravelling doping effects on PEDOT at the molecular level: from geometry to thermoelectric transport properties. J Am Chem Soc 2015;137(40):12929–38.
[30] Dong J, Portale G. Role of the processing solvent on the electrical conductivity of PEDOT:PSS. Adv Mater Interfaces 2020;7(18):2000641.
[31] Bießmann L, Saxena N, Hohn N, Hossain MA, Veinot JGC, Müller-Buschbaum P. Highly conducting, transparent PEDOT:PSS polymer electrodes from post-treatment with weak and strong acids. Adv Electron Mater 2019;5(2):1800654.
[32] Massonnet N, Carella A, Jaudouin O, Rannou P, Laval G, Celle C, et al. Improvement of the Seebeck coefficient of PEDOT:PSS by chemical reduction combined with a novel method for its transfer using free-standing thin films. J Mater Chem C 2014;2(7):1278–83.
[33] Khan ZU, Bubnova O, Jafari MJ, Brooke R, Liu X, Gabrielsson R, et al. Acido-basic control of the thermoelectric properties of poly(3,4-ethylenedioxythiophene)tosylate (PEDOT-Tos) thin films. J Mater Chem C Mater 2015;3(40):10616–23.
[34] Stepien L, Roch A, Schlaier S, Dani I, Kiriy A, Simon F, et al. Investigation of the thermoelectric power factor of KOH-treated PEDOT:PSS dispersions for printing applications. Energy Harvest Syst 2016;3(1):101–11.
[35] Salamat S, Ahsan M, Arif I. Thermoelectric performance of non-degenerate and degenerate semiconductors. In: Proceedings of 2017 Fifth International Conference on Aerospace Science & Engineering (ICASE); 2017 Nov 14–16; Islamabad, Pakistan; 2018. p. 1–5.
[36] Hu Y, Yang R, Evans DF, Weaver JH. Direct measurements of bipolaron-band development in doped polypyrrole with inverse photoemission. Phys Rev B 1991;44(24):13660–5.
[37] Zozoulenko I, Singh A, Singh SK, Gueskine V, Crispin X, Berggren M. Polarons, bipolarons, and absorption spectroscopy of PEDOT. ACS Appl Polym Mater 2019;1(1):83–94.
[38] Xu ZP, Braterman PS. High affinity of dodecylbenzene sulfonate for layered double hydroxide and resulting morphological changes. J Mater Chem 2003;13(2):268–73.
[39] Lefebvre M, Qi Z, Rana D, Pickup PG. Chemical synthesis, characterization, and electrochemical studies of poly(3,4-ethylenedioxythiophene)/poly(styrene-4-sulfonate) composites. Chem Mater 1999;11(2):262–8.
[40] Mitraka E, Jafari MJ, Vagin M, Liu X, Fahlman M, Ederth T, et al. Oxygen-induced doping on reduced PEDOT. J Mater Chem A 2017;5(9):4404–12.
[41] Razmjou A, Asadnia M, Hosseini E, Habibnejad Korayem A, Chen V. Design principles of ion selective nanostructured membranes for the extraction of lithium ions. Nat Commun 2019;10:5793.
[42] Saxena N, Keilhofer J, Maurya AK, Fortunato G, Overbeck J, Müller-Buschbaum P. Facile optimization of thermoelectric properties in PEDOT:PSS thin films through acido-base and redox dedoping using readily available salts. ACS Appl Energy Mater 2018;1(2):336–42.
[43] Anion exchange resin [Internet]. Amsterdam: Elsevier; c2021 [cited 2020 Aug 31]. Available from: https://www.sciencedirect.com/topics/chemistry/anion-exchange-resin.
[44] Sengupta AK. Ion exchange technology advances in pollution control. Boca Raton: CRC Press; 1995.
[45] Guan X, Cheng H, Ouyang J. Significant enhancement in the Seebeck coefficient and power factor of thermoelectric polymers by the Soret effect of polyelectrolytes. J Mater Chem A 2018;6(40):19347–52.
[46] Fan Z, Du D, Guan X, Ouyang J. Polymer films with ultrahigh thermoelectric properties arising from significant Seebeck coefficient enhancement by ion accumulation on surface. Nano Energy 2018;51:481–8.
[47] Ail U, Jafari MJ, Wang H, Ederth T, Berggren M, Crispin X. Thermoelectric properties of polymeric mixed conductors. Adv Funct Mater 2016;26(34):6288–96.